https://doi.org/10.1007/s41230-025-5004-2

Effect of Ta addition on microstructure and mechanical properties of Ti46Al1.5Cr8Nb alloy

Jiang-shan Liang[1], Liao Mi[1], *Hong-ze Fang[1, 2], Xin Ding[1, 2], Xian-fei Ding[3, 5], Bao-hui Zhu[4], and **Rui-run Chen[1, 2]

1. National Key Laboratory for Precision Hot Forming of Metals, Harbin Institute of Technology, Harbin 150001, China

2. Zhengzhou Research Institute, Harbin Institute of Technology, Zhengzhou 450000, China

3. Cast Titanium Alloy R&D Center, Beijing Institute of Aeronautical Materials, Beijing 100095, China

4. Ningxia Horizontal Titanium Industry Co., Ltd., Shizuishan City, Ningxia 753000, China

5. Baimtec Material Co., Ltd., Beijing 100094, China

Abstract: The microstructure of high Nb-TiAl alloys was optimized by the addition of a small amount of Ta elements to further improve their properties. A series of Ti46Al1.5Cr8Nb-*x*Ta (*x*=0.2, 0.4, 0.6, 0.8, 1.0, at.%) alloys were prepared by vacuum arc melting. The microstructure, mechanical properties, and related influencing mechanisms were systematically investigated. The results indicate that the solidification microstructure of the Ti46Al1.5Cr8Nb-*x*Ta alloys comprises the γ-TiAl phase, α_2-Ti_3Al phase, and B2 phase. As the Ta content increases from 0.2at.% to 1.0at.%, the content of α_2 phase and B2 phase increases, while the γ phase content decreases. Among them, the B2 phase shows the most pronounced change, being significantly refined, with its content increasing from 12.49% to 21.91%. In addition, the average size of the lamellar colony decreases from 160.65 to 94.44 μm. The addition of the Ta element shifts the solidification path toward lower aluminum concentrations, leading to changes in phase content. The tantalum-induced increase in the B2 phase and enhanced supercooling at the solidification front provide the basis for lamellar colony refinement. Compressive testing at room temperature reveals that the Ti46Al1.5Cr8Nb0.4Ta alloy exhibits optimal compressive properties, achieving a compressive strength of 2,434 MPa and a compressive strain of 33.1%. The improvement of its properties is attributed to a combination of lamellar colony refinement, solid solution strengthening resulting from the incorporation of Ta element, and a reduction in the *c*/*a* of the γ phase.

Keywords: TiAl alloy; Ta element; microstructure; mechanical properties; lamellar colony

CLC numbers: TG146.23 **Document code:** A **Article ID:** 1672-6421(2026)01-037-08

1 Introduction

TiAl alloys are widely regarded as ideal candidates for structural materials in areas such as aerospace and automotive, owing to their low density, high specific strength, and excellent creep resistance. They have been successfully utilized in components like aero-engine blades and automotive exhaust systems[1-3]. However, limitations in high-temperature performance and room-temperature ductility hinder their broader engineering use[4, 5]. To improve the properties of TiAl alloys, many researchers have attempted to do so by adding alloying elements or improving the preparation process[6-8]. For TiAl alloys exhibiting poor hot workability, low-cost and efficient alloying represents a particularly suitable approach.

The incorporation of high-melting-point Nb elements into TiAl alloys can significantly enhance the high-temperature performance of the alloys. Consequently, high-Nb TiAl alloys are regarded as a new generation of TiAl alloys suitable for higher operating temperatures[9, 10]. In recent years, Ta element as an element belonging to the same VA group as Nb element, has gained increasing attention from researchers due to its higher melting point and superior performance compared to Nb element in

***Hong-ze Fang**

Professor and Doctoral Supervisor. He was selected for the "Youth Talent Support Program" of the China Association for Science and Technology. His research interests mainly focus on electromagnetic cold crucible directional solidification technology; microstructure, property control, and preparation of TiAl alloys and their composites. To date, he has published more than 100 academic papers, and over 30 national invention patents have been granted.

E-mail: fanghongze@hit.edu.cn

****Rui-run Chen**

E-mail: ruirunchen@hit.edu.cn

Received: 2025-01-07; Revised: 2025-03-24; Accepted: 2025-07-01

certain aspects. For example, Lapin et al.[11] compared the microstructures of Ti46Al8Nb and Ti46Al8Ta after directional solidification and found that Ta exhibited better grain-refining effects than Nb in TiAl alloys. Vojtěch et al.[12] found that Ta was more effective than Nb in reducing the oxidation rate of TiAl alloys when comparing the oxidation resistance of Ti-45.2Al-7.2Nb and Ti-44.8Al-6.6Ta alloys. Moreover, Luo et al.[13] found that the addition of an appropriate amount of Ta element can effectively improve the room-temperature plasticity of TiAl alloys. Liu et al.[14] corroborated this finding by preparing Ti48Al2Cr2Nb-*x*Ta alloys using a laser additive manufacturing technique. Their results showed that the addition of 0.5at.% Ta enhanced the room-temperature strength and elongation of the alloys by 1.66 and 1.43 times, respectively, compared to alloys without Ta.

Prior research indicates that the incorporation of Ta element can effectively enhance the properties of TiAl alloys. However, many of these studies have focused on the addition of high Ta content, which is not conducive to the engineering application of TiAl alloys due to the high cost and density of Ta elements. Considering that high Nb-TiAl alloys have a wide range of applications and that Nb and Ta elements have similar chemical properties, therefore, it is a feasible idea to add a small amount of Ta element to high Nb-TiAl alloys to regulate their microstructure and further improve their mechanical properties.

In this work, a small amount of Ta element (0.2at.%–1.0at.%) was added to Ti46Al1.5Cr8Nb alloy. The changes in microstructure and room-temperature compressive properties with varying Ta content were comparatively analyzed to reveal the effects of a small amount of Ta element addition on the evolution of the microstructure and mechanical properties of the Ti46Al1.5Cr8Nb alloy. The underlying mechanism was further explored.

2 Experimental methods

Ti46Al1.5Cr8Nb-*x*Ta (*x*=0.2, 0.4, 0.6, 0.8, 1.0, at.%) alloys, named as 0.2Ta, 0.4Ta, 0.6Ta, 0.8Ta, 1.0Ta, were prepared by vacuum arc melting under an argon atmosphere. Following high-purity raw materials were used: Al (99.99wt.%), Cr (99.9wt.%), Ta (99.9wt.%), Al-Nb master alloy (70wt.% Nb), and Ti (99.7wt.%). The raw materials were sequentially added into the crucible in the aforementioned order. The resulting button ingot was weighed 80 g with a diameter of 50 mm and a thickness of 10 mm. To ensure uniform solidification, each ingot was melted four times during the preparation process.

The button ingot was cut along the centerline, and a 10 mm×10 mm×10 mm sample was extracted for phase constitution analysis using X-ray diffraction (XRD). After polishing, the sample was etched with a solution containing 10vol.% HNO_3, 5vol.% HF, and 85vol.% H_2O for 4–6 s for microstructural observation. The macroscopic and microstructural features of the alloys were observed using a Quanta200F scanning electron microscope (SEM). B2 phase content and lamellar colony size were measured using Image Pro software. At least five SEM images were selected to calculate the content of B2 phase and other phases based on their color contrast, with the average value taken. The size of the lamellar colonies was determined using the intercept method. The elemental distributions were analyzed using energy-dispersive spectroscopy (EDS).

Room-temperature compressive properties were tested using an AG-X Plus 250 kN/50 kN testing machine at a loading rate of 0.5 mm·min^{-1}. To ensure experimental repeatability, three cylindrical samples (Φ4 mm×6 mm) were cut from the button ingots for testing.

3 Results

3.1 Phase analysis of Ti46Al8Nb1.5Cr-*x*Ta alloys

Figure 1(a) presents the XRD phase analysis of the Ti46Al8Nb1.5Cr-*x*Ta alloys. The XRD patterns reveal that Ti46Al8Nb1.5Cr-*x*Ta alloys are composed of γ-TiAl, α_2-Ti_3Al, and B2 phases. The diffraction peaks are dominated by the γ phase and the peak at $(111)_\gamma$ is the strongest, indicating that the γ phase is the matrix phase of Ti46Al8Nb1.5Cr-*x*Ta alloys. The diffraction peaks of the α_2 phase are observed only at 35.90°, 41.09°, and 78.07°. The intensity of the α_2 phase diffraction peak at 78.07° gradually increases with the increase of Ta content, indicating that its relative content gradually increases. In addition, the diffraction peak of the B2 phase appears at 70.28° when the Ta content is 1.0at.%, indicating that the addition of Ta promotes the formation of B2 phase, which is generally considered detrimental to the alloy's properties.

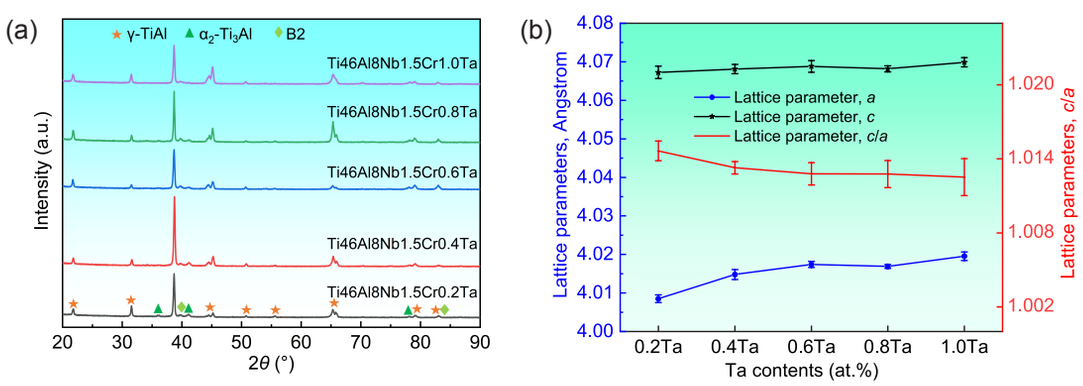

Fig. 1: XRD results of Ti46Al8Nb1.5Cr-*x*Ta alloy: (a) phase constitution; (b) *γ* phase lattice parameter

The lattice constant of the matrix γ phase was further calculated using Jade software, and the results are presented in Fig. 1(b). The lattice parameter *a* of the γ phase exhibits a slight increase with increasing Ta content, while the value of *c* remains approximately constant at 4.068. Consequently, the *c*/*a* ratio of the γ phase in the alloy decreases marginally. γ phase is an L10-type crystal structure that exhibits asymmetric features. As the Ta content increases, the *c*/*a* value of the γ phase in the Ti46Al8Nb1.5Cr-*x*Ta alloy decreases, the symmetry of the crystal structure improves.

3.2 Solidification structure characteristics of Ti46Al8Nb1.5Cr-*x*Ta alloys

Figure 2 shows the solidification structure characteristics of the Ti46Al8Nb1.5Cr-*x*Ta alloy. The microstructure consists of grey (α_2+γ) lamellae, bright white B2 phase, and a small amount of dark block γ phase. A significant portion of the B2 phase is distributed along the (α_2+γ) lamellae, while a smaller amount is present between adjacent lamellar colonies. The B2 phase exhibits a morphology of long-strip-shaped or a network within the microstructure. As the Ta content increases, the solidification microstructure undergoes two notable changes. On the one hand, both the size and number of B2 phases in the alloy change. As illustrated in Fig. 3(a), the B2 phase content increases from 12.49% to 21.91% as the Ta content rises from 0.2at.% to 1.0at.%. Moreover, when the Ta content exceeds 0.4at.%, the size of the B2 phase decreases significantly, and it exhibits a more pronounced network morphology. This indicates that Ta, as a β stabilizing element, can influence the microstructure of TiAl alloys by affecting the formation and distribution of the B2 phase.

On the other hand, the (α_2+γ) lamellar colony of Ti46Al8Nb1.5Cr-*x*Ta alloys is refined with increasing Ta content. The average lamellar colony size of the alloy was measured using statistical methods, and the results are presented in Fig. 3(b). As the Ta content increases from 0.2at.% to 1.0at.%, the average lamellar colony size decreases from 160.65 to 94.44 μm. This indicates that the addition of the Ta element refines the (α_2+γ) lamellar colony of TiAl alloys.

3.3 Element distribution of Ti46Al8Nb1.5Cr-*x*Ta alloys

The element distribution of Ti46Al8Nb1.5Cr-*x*Ta alloys was analyzed using EDS. Measurements were primarily taken at two locations: the (α_2+γ) lamellae colony and the B2 phase. The selected point positions are illustrated in Fig. 4, where Point 1 represents the (α_2+γ) lamellae colony and Point 2 represents the B2 phase. The quantitative results of the point scans are presented in Table 1. The EDS results indicate that, compared

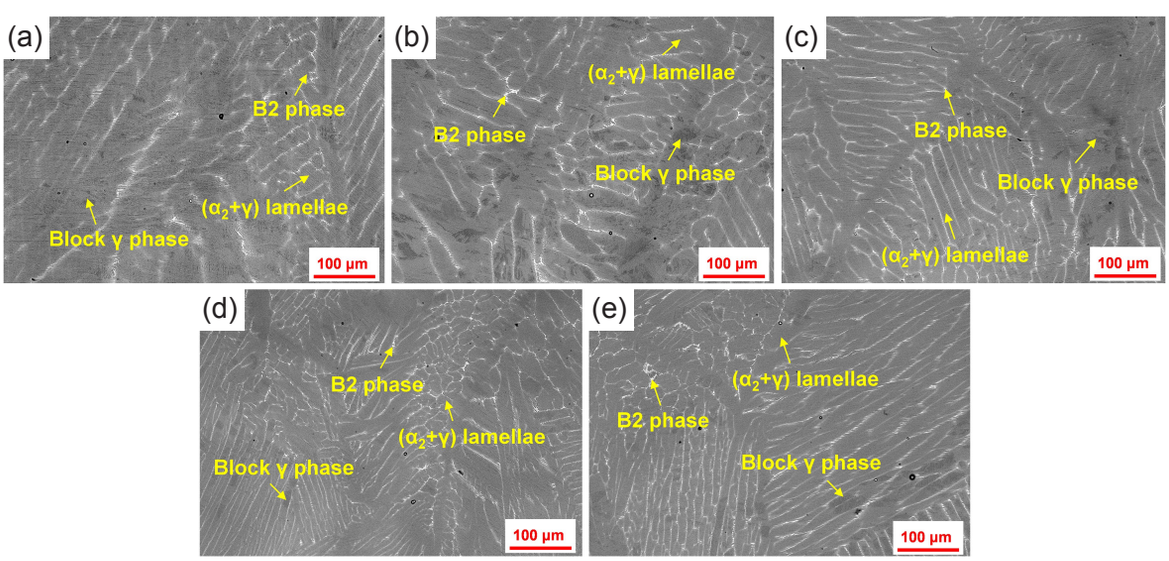

Fig. 2: Solidification structure of Ti46Al8Nb1.5Cr-*x*Ta alloys: (a) 0.2Ta; (b) 0.4Ta; (c) 0.6Ta; (d) 0.8Ta; (e) 1.0Ta

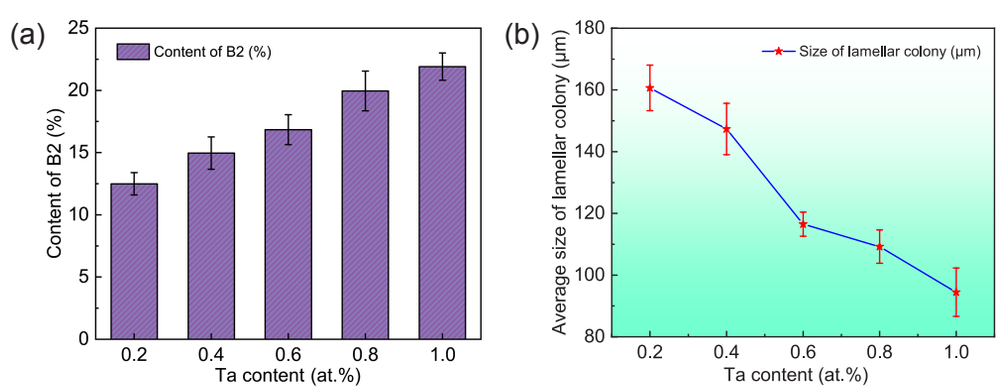

Fig. 3: B2 phase content and average size of lamellar colony in Ti46Al8Nb1.5Cr-*x*Ta alloys: (a) B2 phase content; (b) average size of lamellar colony

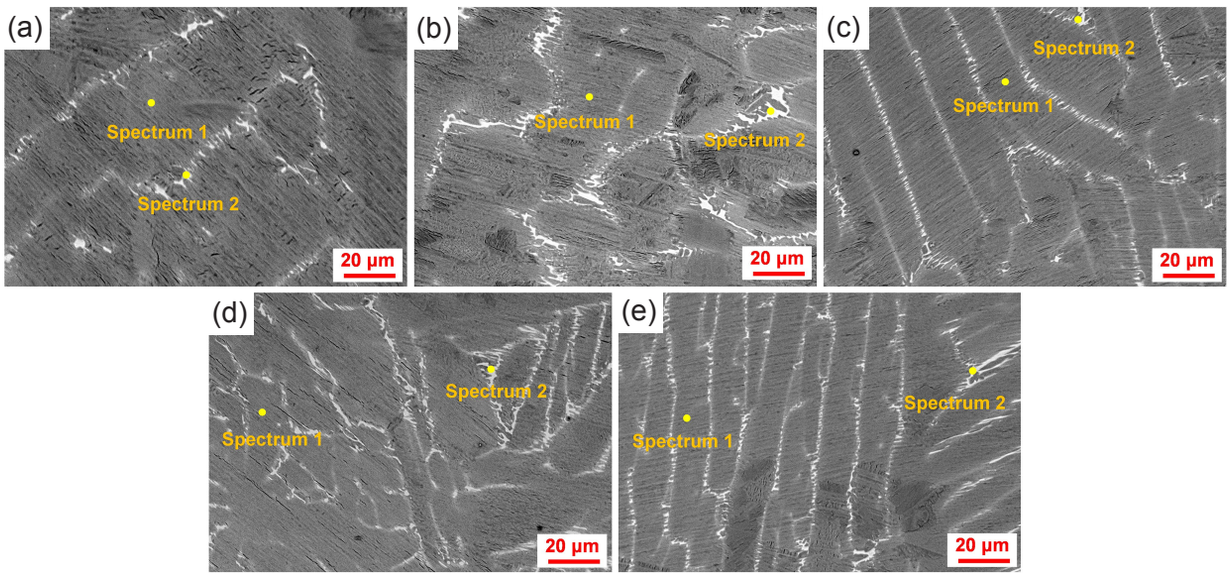

Fig. 4: Solute distribution of Ti46Al8Nb1.5Cr-*x*Ta alloy: (a) 0.2Ta; (b) 0.4Ta; (c) 0.6Ta; (d) 0.8Ta; (e) 1.0Ta

Table 1: Results of solute distribution of Ti46Al8Nb1.5Cr-*x*Ta alloys (at.%)

Ti46Al8Nb 1.5Cr-*x*Ta	Point	Al	Ti	Cr	Nb	Ta
0.2Ta	1	45.05	45.55	1.37	7.90	0.13
	2	37.50	50.14	3.00	9.07	0.29
0.4Ta	1	45.42	45.69	1.18	7.43	0.28
	2	41.82	46.72	2.37	8.72	0.37
0.6Ta	1	44.06	46.36	1.48	7.61	0.49
	2	42.49	46.05	2.23	8.59	0.64
0.8Ta	1	44.42	46.02	1.42	7.54	0.61
	2	39.72	48.10	2.88	8.36	0.94
1.0Ta	1	45.47	44.84	1.24	7.60	0.86
	2	41.05	47.19	2.36	8.40	1.00

to the (α_2+γ) lamellae colony, the B2 phase lacks Al atoms and is enriched with a large number of Cr atoms as well as a small amount of Nb and Ta atoms. This is attributed to the fact that Al is an α-stabilizing element, whereas Nb, Cr, and Ta are β-stabilizing elements, which tend to segregate to the B2 phase. With increasing Ta content, the solubility of Ta atoms increases in both the (α_2+γ) lamellar colony and the B2 phase. The solubility limit of Ta atoms in (α_2+γ) lamellae colony is not reached even when the Ta element is added at 1.0at.%. Furthermore, it is observed that the Nb content in the B2 phase tends to decrease.

3.4 Mechanical properties of Ti46Al8Nb1.5Cr-*x*Ta alloys

The compressive properties of Ti46Al8Nb1.5Cr-*x*Ta alloys at room temperature are shown in Fig. 5. Among these alloys, Ti46Al8Nb1.5Cr0.4Ta alloy exhibits the best compressive properties. As shown in Fig. 5, the alloys demonstrate a consistent trend of change in both compressive strength and compressive strain with increasing Ta content. Specifically, as the Ta content increases from 0.2at.% to 0.4at.%, the

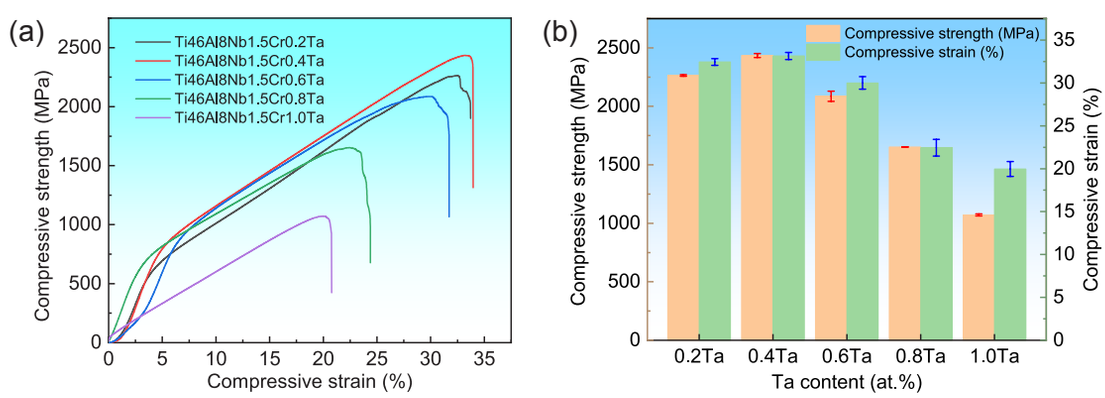

Fig. 5: Compressive properties of Ti46Al8Nb1.5Cr-*x*Ta alloy: (a) compressive stress-strain curve; (b) compressive stress-strain histogram

compressive strength increases from 2,263 to 2,434 MPa, and the compressive strain increases from 32.4% to 33.1%. Subsequently, when the Ta content is increased from 0.4at.% to 1.0at.%, both the compressive strength and compressive strain decrease, from 2,434 to 1,071 MPa and 33.1% to 20.0%, respectively. Furthermore, the compressive properties of the Ti46Al8Nb1.5Cr0.4Ta alloy are compared with those of TiAl alloys reported in recent years, as presented in Fig. 6. This comparison reveals that the compressive properties of the designed Ti46Al8Nb1.5Cr0.4Ta alloy are at a high level.

Figures 7(a) and (b) display the microstructures of the alloy near the room-temperature compression crack for Ta additions of 0.4at.% and 1.0at.%. The Ti46Al8Nb1.5Cr0.4Ta alloy

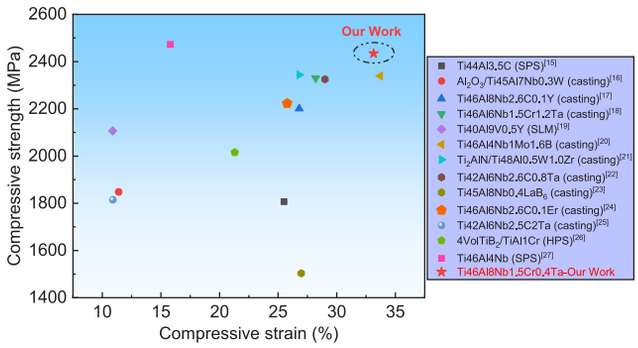

Fig. 6: Comparison of compression properties of TiAl alloys in recent years

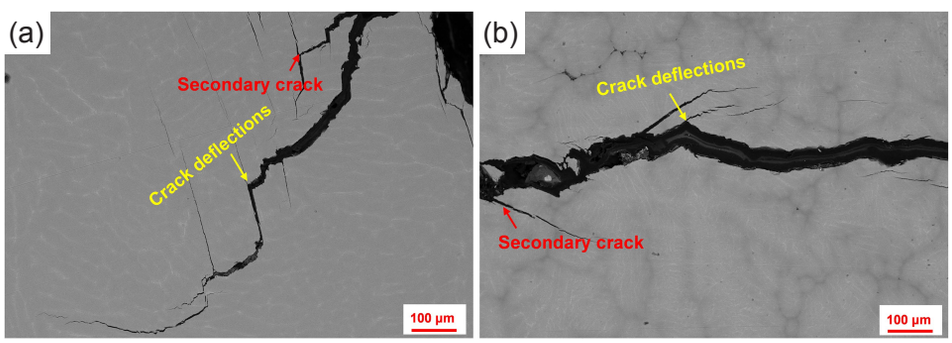

Fig. 7: Microstructures of alloy near room-temperature compression crack: (a) 0.4Ta; (b) 1.0Ta

exhibits a narrower crack width, with multiple crack deflections occurring during crack propagation. These crack deflections increase the propagation path, dissipate additional energy, and reduce the crack growth rate, thereby enhancing the alloy's compressive strength. Furthermore, secondary cracks are observed near the primary crack. They can also absorb a portion of the energy. Conversely, the Ti46Al8Nb1.5Cr1.0Ta alloy shows a relatively straight crack with a handful deflection. This indicates that the Ti46Al8Nb1.5Cr1.0Ta alloy only needs to consume a small amount of energy to allow the cracks to expand further, which is detrimental to the strength of the alloy. The observed crack propagation behavior further indicates that the Ti46Al8Nb1.5Cr0.4Ta alloy possesses better properties.

4 Discussion

4.1 Influencing mechanism of Ta on solidification microstructure

The solidification path dictates the formation of the final solidified microstructure in TiAl alloys. The addition of Nb, Ta, and Cr inevitably alters the solidification path of the Ti46Al alloy. To elucidate the mechanism by which Ta element influences the solidification microstructure, the equivalent Al content was firstly calculated using the Al-equivalent method to determine the equilibrium solidification path of Ti46Al8Nb1.5Cr-xTa alloys. The corresponding calculation equations are presented in Eqs. (1) and (2):

$$C_i'=C_i/(100-C_x)(i=\text{Ti or Al},\ x=\text{Nb}+\text{Cr}+\text{Ta}+\ldots) \quad (1)$$

$$C_{\text{Al}}''=C_{\text{Al}}-(a\cdot X_{\text{Al-eq}}+b\cdot Y_{\text{Al-eq}}+c\cdot Z_{\text{Al-eq}}) \quad (2)$$

where C_i' is the atomic percentage content of Ti or Al after removal of the elements Nb, Cr, and Ta. C_i is the atomic percentage of Ti or Al, and C_x is the atomic percentage of Nb, Cr, and Ta. C''_{Al} is the equivalent of Al and $X_{\text{Al-eq}}$, $Y_{\text{Al-eq}}$, and $Z_{\text{Al-eq}}$ refer to the equivalent Al equivalents of the elements Nb, Cr, and Ta, respectively. Where $X_{\text{Al-eq}}$ is +0.3, $Y_{\text{Al-eq}}$ is +0.1, and $Z_{\text{Al-eq}}$ is +0.3[28]. The specific calculations of Al equivalents are given in Table 2.

The calculation results in Table 2 show that the addition of Nb, Cr, and Ta elements has a greater influence on its solidification path. Combined with the phase diagram of TiAl alloys, it is judged that its equilibrium solidification path is roughly as follows: L→L+β→β→β+α→α→α+γ→α_2+γ. Under equilibrium conditions, the Ti46Al8Nb1.5Cr-xTa alloys

Table 2: Calculation of Al equivalent under different Ta contents

Ta content (at.%)	C''_{Al} (%)
0.2	48.33
0.4	48.38
0.6	48.44
0.8	48.49
1.0	48.55

would solidify following the solidification pathway described previously. The initial phase of the solidification process is the β phase. However, due to the fast solidification rate of arc melting, the primary β phase does not fully transform into the α phase. Instead, it directly enters the single-phase α region. These untransformed β phases are then distributed along the grain boundaries of the α phase, ultimately forming the B2 phase between adjacent lamellar colonies. Subsequently, during the $\alpha \rightarrow \alpha_2+\gamma$ transformation, the Nb, Cr, and Ta become further enriched in the α phase, ultimately leading to the formation of the B2 phase along the $(\alpha_2+\gamma)$ lamellar. Furthermore, the incorporation of Cr inhibits α-transformation during this process, leading to the coarsening of the γ phase and its transformation into a block γ phase[29]. Consequently, the final solidified microstructure of Ti46Al8Nb1.5Cr-*x*Ta alloys comprises $(\alpha_2+\gamma)$ lamellae, block γ phase, and the B2 phase. Figure 8 shows the schematic diagram of the solidification path of Ti46Al8Nb1.5Cr-*x*Ta alloys.

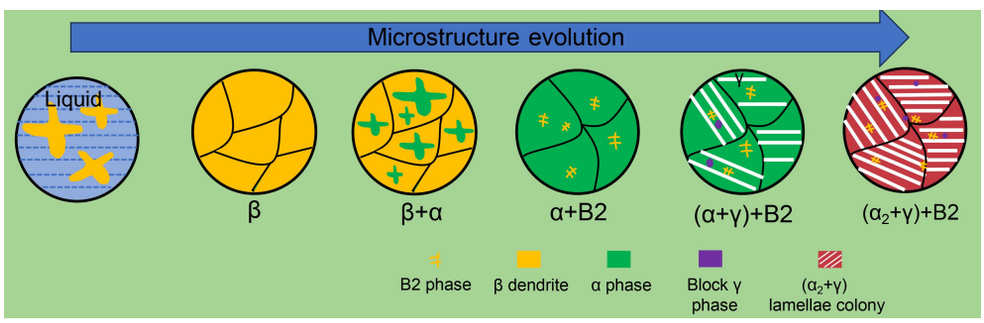

Fig. 8: Schematic diagram of solidification path for Ti46Al8Nb1.5Cr-*x*Ta alloys

The calculated Al equivalents in Table 2 indicate that the solidification path shifts toward lower Al content as the Ta content increases, aligning with the findings of Duan et al[30]. The binary TiAl phase diagram indicates that a decrease in Al content enhances the proportion of the α_2 phase and reduces the proportion of the γ phase. Furthermore, studies demonstrate that adding Ta increases the liquid-phase transition temperature of TiAl alloys[31]. As a β-phase stabilizing element, Ta lowers the β-phase transition temperature, allowing the β-phase to exist at lower temperatures and thereby expanding its stable temperature range. Consequently, Ta addition enlarges the L+β phase region and promotes the formation of β phases, leading to a higher B2 phase content in the solidified microstructure. Thus, as Ta content rises, the amounts of α_2 phase and B2 phase in the solidified microstructure increase, whereas the γ phase decreases.

The formation of B2 phase is closely associated with the high-temperature β phase. As β-stabilizing elements, Nb and Ta tend to concentrate in the β phase during solidification. Compared to Nb, Ta has a higher melting point and a lower diffusion rate. As the Ta content increases, more Ta atoms incorporate into the β phase, impeding Nb diffusion into this phase. Additionally, research indicates that Ta atoms can replace Nb atoms in TiAl alloys, thereby promoting the dispersion of Nb in the matrix[18]. Consequently, the Nb concentration in the B2 phase decreases with increasing Ta content, which aligns with the elemental distribution observed in Table 1.

In TiAl alloys that follow the β-solidification path, the size of the initial β phase determines the resulting $(\alpha_2+\gamma)$ lamellar colony size[10]. As the Ta content increases, more Ta atoms, which have a high melting point, accumulate at the solidification front. This results in greater supercooling at the solidification front, promoting the nucleation of the initial β-phase while inhibiting its subsequent growth. Additionally, Ta atoms, characterized by high melting points, large atomic radii, and low diffusion coefficients, become enriched in the β phase. This enrichment hinders the diffusion of other atoms, further refining the β phase. Moreover, the B2 phase, distributed between adjacent lamellar colonies, restricts the growth of the $(\alpha_2+\gamma)$ lamellae colony. An increase in the B2 phase also contributes to the refinement of the $(\alpha_2+\gamma)$ lamellar colony in Ti46Al8Nb1.5Cr-*x*Ta alloys. Consequently, these factors collectively reduce the lamellar colony size of the alloy as the Ta content increases.

4.2 Effect of Ta element on mechanical properties of alloys

Fine-grain reinforcement plays an important role in this study. As shown in Fig. 3(b), Ta additions refine the $(\alpha_2+\gamma)$ lamellar colonies. The relationship between the strength (σ_y) and the lamellar colony size of TiAl alloys satisfies the Hall-Petch relationship:

$$\sigma_y = \sigma_0 + K_y d_i^{-1/2} \quad (3)$$

where σ_0 is 242.98 MPa, K_y is the grain boundary strengthening coefficient of 4.8 MPa·m$^{-1/2}$[32], and d_i represents the average lamellar colony size. According to the above equation, the average lamellar colony size of Ti46Al8Nb1.5Cr-*x*Ta alloys gradually decreases with the increase of Ta element content in the alloy, which is favorable to the strength of the alloy. The results of the calculations are shown in Fig. 9. It can be seen that σ_y increases with the increase of Ta. This is because the addition of Ta leads to the refinement of lamellar colonies. Furthermore, Fang et al.[17] reported that refined $(\alpha_2+\gamma)$ lamellar colonies in TiAl alloys promote a more homogenous microstructure, which enables the stresses caused by local deformation to be distributed to each lamellar colony, thereby mitigating stress concentrations and enhancing mechanical properties.

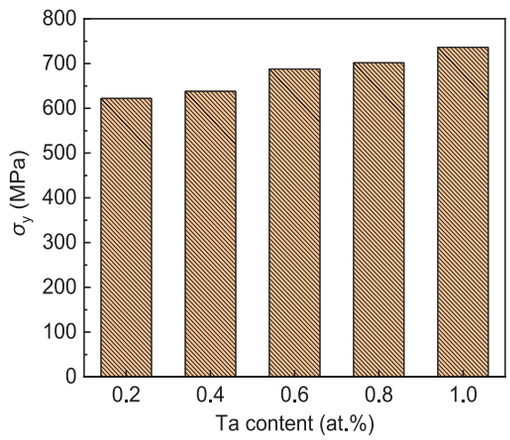

Fig. 9: Calculation of σ_y based on Eq. (3)

Solid solution strengthening is not negligible in this study. The effect of solid solution strengthening is influenced by the concentration of solute atoms and the size difference between solute and solvent atoms. In TiAl alloys, Ta atoms primarily replace Ti atoms in lamellar colonies[33], where a size mismatch exists between Ta atoms (149 pm) and Ti atoms (146 pm). The incorporation of larger Ta atoms into the matrix induces lattice distortion, which hinders dislocation motion and enhances the alloy's strength. The solid solution strengthening effect ($\Delta\sigma_{ss}$) can be expressed by considering the dislocation-solute elastic interaction, as described by Eq. (4):

$$\Delta\sigma_{ss} = \left(\sum\nolimits_i B_i^{3/2} x_i\right)^{2/3} \quad (4)$$

where B_i represents the strengthening coefficient of each element group, and x_i denotes the solute concentration. As the Ta content increases, the concentration of Ta atoms dissolved in the lamellar colony rises, further amplifying the strengthening effect.

The preceding analysis indicates that both fine-grain strengthening and solid-solution strengthening contribute to the enhanced properties of Ti46Al8Nb1.5Cr-*x*Ta alloys. Furthermore, XRD analysis reveals that increasing Ta content reduces the *c*/*a* of the γ phase. The γ phase is the primary source of plastic deformation in TiAl alloys[34]. Therefore, the decrease of the *c*/*a* of the γ phase is conducive to the improvement of the alloy deformation capacity. However, with increasing Ta content, the amount of the B2 phase in the microstructure increases, and its morphology undergoes significant changes. Particularly, when the Ta content exceeds 0.4at.%, the quantity of the B2 phase in the alloy increases, and its distribution within the matrix becomes denser, which severely impairs the alloy's performance. On the one hand, the slip systems of the B2 phase are insufficient, making it difficult to deform at room temperature. It often becomes a point of stress concentration due to its poor compatibility with the matrix during deformation[35,36]. When stress concentration cannot be alleviated through continuous slip or other deformation mechanisms, cracks may form at the interface or within the B2 phase, leading to alloy failure. On the other hand, as the Ta content increases, the B2 phase exhibits a more pronounced network distribution, further segmenting the (α_2+γ) lamellar structure. This also adversely affects the alloy's performance. Lee believes that a large amount of B2 phase disrupts the overall integrity of the lamellar structure, which is a significant factor contributing to the overall decline in the alloy's performance[37]. The reasons mentioned above lead to a decrease in the alloy's performance when the Ta content exceeds 0.4at.%. Consequently, the Ti46Al8Nb1.5Cr0.4Ta alloy exhibits the optimal performance.

5 Conclusions

The Ti46Al8Nb1.5Cr alloy was selected to improve its microstructure and mechanical properties by adding a small amount of the element Ta (0.2at.%–1.0at.%). The effects of varying Ta content on phase constitution, solidification microstructure, elemental distribution, and room-temperature compressive properties were examined. The main conclusions are summarised below:

(1) The solidification microstructure of Ti46Al1.5Cr8Nb-*x*Ta alloys consists of (α_2+γ) lamellae, block γ phase, and B2 phase. Increasing Ta content promotes the formation of α_2 and B2 phases. This change is attributed to the influence of Ta on the solidification path, shifting it toward the lower Al region and expanding the L+β phase region.

(2) Increasing the Ta content refines the alloy's lamellar colony, reducing the average lamellar colony size from 160.65 to 94.44 μm. The addition of the Ta element increases the constitutional undercooling on the solidification front. This inhibits β phase growth, refining the lamellar colonies. Furthermore, the increased B2 phase also contributes to lamellar colony refinement.

(3) The room temperature compressive properties of the Ti46Al8Nb1.5Cr-*x*Ta alloys show an increasing and then decreasing trend. The best performance of the alloy is obtained when the Ta content is 0.4at.%, with a compressive strength of 2,434 MPa and a compressive strain of 33.1%.

(4) The enhancement of alloy properties is attributed to several factors: the refinement of the lamellar colony, solid solution strengthening induced by Ta element, and a reduction in the *c*/*a* of the γ phase.

Acknowledgments

The authors are grateful to the financial support by the Major Science and Technology Achievement Transformation Project in Heilongjiang Province (No. ZC2023SH0075), the National Natural Science Foundation of China (Nos. 52425401, U2441255, 52474377, and 52371015), the Young Elite Scientists Sponsorship·Program by CAST (No. 2021QNRC001), and the Henan Provincial Key Research and Development & Promotion Special Program (No. 251111231400).

Conflict of interest

Prof. Rui-run Chen is an EBM of *CHINA FOUNDRY*. He was not involved in the peer-review or handling of the manuscript. The authors have no other competing interests to disclose.

References

[1] Han J C, Dong J, Zhang S Z, et al. Microstructure evolution and tensile properties of conventional cast TiAl based alloy with trace Ni addition. Materials Science & Engineering: A, 2018, 715: 41–48.
[2] Bewlay B, Nag S, Suzuki A, et al. TiAl alloys in commercial aircraft engines. Materials at High Temperatures, 2016, 33(4–5): 549–559.
[3] Zheng G, Tang B, Zhao S, et al. Evading the strength-ductility trade-off at room temperature and achieving ultrahigh plasticity at 800 °C in a TiAl alloy. Acta Materialia, 2022, 225: 117585.
[4] Liang H, Ding H S, Xu X S, et al. Effect of variation in Zr content on microstructure and high-temperature tensile properties of a γ-TiAl alloy. Materials Science & Engineering: A, 2024, 893: 146085.
[5] Wang K G, Tian Y Y, Deng Z X, et al. Effects of boron, Hf and Ta content on boride morphology and microstructure of β-solidified γ-TiAl alloys. Vacuum, 2023, 215: 112363.
[6] Clemens H, Mayer S. Design, processing, microstructure, properties, and applications of advanced intermetallic TiAl alloys. Advanced Engineering Materials, 2013, 15: 191–215.
[7] Raji S A, Popoola A P I, Pityana S L, et al. Characteristic effects of alloying elements on β solidifying titanium aluminides: A review. Heliyon, 2020, 6(7): e04463.
[8] Xu R R, Li M Q, Zhao Y H. A review of microstructure control and mechanical performance optimization of γ-TiAl alloys. Journal of Alloys and Compounds, 2023, 932: 167611.
[9] Zhang W J, Chen G L, Sun Z Q. Oxidation of ternary Ti18Nb48Al and Ti10Nb45Al alloys. Scripta Metallurgica et Materialia,1993, 28(5): 563–567.
[10] Cao J, Sun T L, Guo Z C, et al. Simultaneous enhancement of strength and ductility in high Nb-TiAl by Si alloying. Journal of Materials Science & Technology, 2024, 177: 128–132.
[11] Lapin J, Marek K. Effect of continuous cooling on solid phase transformations in TiAl-based alloy during Jominy end-quench test. Journal of Alloys and Compounds, 2018, 735: 338–348.
[12] Vojtěch D, Popela T, Kubásek J, et al. Comparison of Nb- and Ta-effectiveness for improvement of the cyclic oxidation resistance of TiAl-based intermetallics. Intermetallics, 2011, 19(4): 493–501.
[13] Luo Y Y, Zeng W D, Xi Z P, et al. Microstructure, mechanical properties and oxidation behavior of a hot-extruded TiAl containing Ta. Rare Metal Materials and Engineering, 2015, 44(2): 282–287.
[14] Liu Z Q, Wang C Y, Wang W B, et al. Effects of Tantalum on the microstructure and properties of Ti-48Al-2Cr-2Nb alloy fabricated via laser additive manufacturing. Materials Characterization, 2021, 179: 111317.
[15] Liu P, Hou B, Wang A Q, et al. Balancing the strength and ductility of Ti AlC/TiAl composite with a bioinspired micro-nano laminated architecture. Materials & Design, 20222, 20: 110851.
[16] Lu X F, Li J B, Chen X H, et al. Grinding mechanism and mechanical properties of the in-situ synthesized Al_2O_3/TiAl composites. Ceramics International, 2019, 45(9): 12113–12121.
[17] Fang H Z, Li K X, Chen R R, et al. Refining Ti_2AlC in the liquid region and improving the microstructure and mechanical properties of Ti-46Al-8Nb-2.6C alloy by adding Y. Journal of Alloys and Compounds, 2024, 982: 173799.
[18] Zhou L Y, Fang H Z, Yang X K, et al. Adjusting the γ/α_2 and Ti_2AlC phase on microstructure evolution and improving mechanical properties at room and elevated temperatures with the addition of Ta. Intermetallics, 2022, 146: 107579.
[19] Gao P, Huang W P, Yang H H, et al. Cracking behavior and control of β-solidifying Ti-40Al-9V-0.5Y alloy produced by selective laser melting. Journal of Materials Science & Technology, 2020, 39: 144–154.
[20] Tan Y M, Chen R R, Fang H Z, et al. Enhanced strength and ductility in Ti46Al4Nb1Mo alloys via boron addition. Journal of Materials Science & Technology, 2022, 102: 16–23.
[21] Chen S Y, Tan Y M, Wang X, et al. Comparing the role of Zr and Hf atoms on microstructure and mechanical properties optimization of Ti_2AlN reinforced Ti48Al0.5W composites. Journal of Alloys and Compounds, 2023, 935: 168159.
[22] Fang H Z, Chen R R, Chen X Y, et al. Effect of Ta element on microstructure formation and mechanical properties of high-Nb TiAl alloys. Intermetallics, 2019, 104: 43–51.
[23] Fang Y C, Jin K H, Liu C, et al. Effect of LaB_6 on the microstructure evolution and mechanical properties of Ti-45Al-8Nb alloy. Journal of Alloys and Compounds, 2023, 938: 168513.
[24] Fang H Z, Li K X, Chen R R, et al. Refining Ti_2AlC particles and improvement of microstructure and mechanical properties on Ti46Al8Nb2.6C alloy by Er addition. Materials Science & Engineering: A, 2022, 857: 144012.
[25] Fang H Z, Yang X K, Zhou L Y, et al. Exploration of homologous substitution element on phase ratio and high temperature properties in high Nb-containing TiAl alloy. Journal of Alloys and Compounds, 2022, 918: 165782.
[26] Wei Y Z, Qiu F, Shu S L, et al. Microstructure manipulation and strengthening mechanism of TiAl composites reinforced by Cr solid solution and in-situ nanometer-sized TiB_2 particles. Materials Science & Engineering: A, 2022, 845: 143214.
[27] Yang S C, Cui C X, Cui S, et al. Microstructure and mechanical properties of in-situ dual morphology Ti_8C_5/TiB_2 reinforced TiAl composite. Materials Science & Engineering: A, 2022, 840: 142918.
[28] Johnson D R, Inui H, Muto S, et al. Microstructural development during directional solidification of a-seeded TiAl alloys. Acta Materialia, 2006, 54(4): 1077–1085.
[29] Xu X S, Ding H S, Huang H T, et al. Microstructure and elevated temperature tensile property of Ti-46Al-7Nb-(W,Cr,B) alloy compared with binary and ternary TiAl alloy. Materials Science & Engineering: A, 2021, 807: 140902.
[30] Duan B H, Yang Y C, He S Y, et al. History and development of γ-TiAl alloys and the effect of alloying elements on their phase transformations. Journal of Alloys and Compounds, 2022, 909: 164811.
[31] Shuleshova O, Holland-Moritz D, Voss A, et al. In situ observations of solidification in Ti-Al-Ta alloys by synchrotron radiation. Intermetallics, 2011, 19(5): 688–692.
[32] Yang S C, Cui C X, Cui S, et al. Ti-46Al-4Nb alloy refined and reinforced by insitu TiC nanoparticles and TiB_2 whiskers. Journal of Alloys and Compounds, 2022, 892: 162195.
[33] Hao Y L, Yang R, Cui Y Y, et al. The effect of Ti/Al ratio on the site occupancies of alloying elements in γ-TiAl. Intermetallics, 2000, 8(5–6): 633–636.
[34] Hao Y J, Liu J X, Li S K, et al. Effects of nano-twinning on the deformation and mechanical behaviours of TiAl alloys with distinct microstructure at elevated loading temperatures. Materials Science & Engineering: A, 2017, 705: 210–218.
[35] Ding H S, Wang Y Z, Chen R R, et al. Effect of growth rate on microstructure and tensile properties of Ti-45Al-2Cr-2Nb prepared by electromagnetic cold crucible directional solidification. Materials and Design, 2015, 86: 670–678.
[36] Xu X S, Ding H S, Huang H T, et al. Twinning-induced dislocation and coordinated deformation behavior of a high-Nb TiAl alloy during high-cycle fatigue. International Journal of Fatigue, 2023, 171: 107597.
[37] Lee H N, Johnson D R, Inui H, et al. Microstructural control through seeding and directional solidification of TiAl alloys containing Mo and C. Acta Materialia, 2000, 48(12): 3221–3233.